Journal of Materials Chemistry A

ROYAL SOCIETY OF CHEMISTRY

PAPER

Published on 13 July 2021
Licence and permissions

Cite this: *J. Mater. Chem. A*, 2021, **9**, 16974

Photothermal slippery surfaces towards spatial droplet manipulation†

Keyu Han,‡[a] Zubin Wang, ‡[b] Liping Heng *[a] and Lei Jiang [a]

Intelligent responsive slippery surfaces with adjustable wettability have considerable significance in a broad range of fundamental research and application realms including microfluidic channels, microreactions, and liquid directional-conveying devices. Although considerable progress has been made in current responsive slippery surfaces, most of them usually function under a contact-type stimulus with restricted operating conditions or constructing responsivity in the whole surface, which have difficulty in satisfying remote and flexible responsive demands in complicated practical environments. Therefore, designing slippery surfaces with a configurable wettability pattern and spatial response to remote stimuli is especially important, which remains a significant challenge. Herein, we present a photothermal ZnO–Pt–fluoroalkylsilane (FAS)–paraffin slippery surface (ZPFPSS) with sensitive light responsiveness. Owing to Pt's photothermal characteristic, the paraffin layer in the ZPFPSS switched between the solid and the liquid state under on–off irradiation. This endowed the ZPFPSS with reversible switching slippery property between the pinning state and easy-sliding state for different liquid droplets. In addition, versatile responsive pathways were designed, achieving spatial manipulation of the droplets. Meanwhile, programmable micro-droplet storage with rewritable property was also achieved on the ZPFPSS. This work provides a promising interface with responsive pathways, promoting its potential applications in rewritable functional biochips, microfluidics and water-harvesting systems.

Received 19th May 2021
Accepted 9th July 2021

DOI: 10.1039/d1ta04243b

rsc.li/materials-a

Introduction

Specific wettability surfaces inspired by organism constructions have aroused extensive attention due to their broad technological potential in various fields of environment, energy, and health.[1–3] As an excellent paradigm among them, slippery liquid-infused porous surfaces (SLIPSs) inspired by the *Nepenthes* pitcher plant demonstrated state-of-the-art properties, such as a stable and omniphobic character towards various simple and complex mixed liquids.[4–7] Especially, as emerging representatives of functional interfaces, responsive SLIPSs have been progressively developed for intelligently regulating droplet motion under various external single stimuli such as mechanical forces,[8] magnetic field,[9,10] temperature[11,12] and electric field,[5,13–15] or even dual photoelectric cooperative-stimuli.[16,17] Owing to their excellent stain-resistance, icephobic features, and intelligent responsiveness, responsive SLIPSs have widespread applications in the fields of liquid and bubble manipulation,[9,18–20] anti-icing,[21] dropwise collection,[22,23] microfluidic channels,[24] and patterned writing.[17] SLIPSs' responsiveness is derived from their unique responsive substrates, such as porous elastomer membranes,[25,26] magnetic cone arrays,[27,28] composite photoelectric sensitization films[17] and electrostrictive polymers,[29,30] or their responsive lubricant like magnetic fluid, paraffin with temperature phase change and ionic liquid with conductivity.[31,32] For instance, Hu's group[29] reported a slippery surface by combining poroelastic film and silicone oil. This slippery surface could be regulated by programmed voltages, thus controlling the liquid droplet sliding behaviours. Seimei Shiratori's group[33] constructed a temperature-activated slippery surface based on paraffin and hydrophobic porous film, on which the droplet sliding behaviour and surface light transmittance was regulated in response to the temperature change. Varanasi *et al.*[34] demonstrated a slippery surface filled with ferrofluid, which enabled manipulation of the droplet using a magnetic field.

Although significant advancements in the fields of responsive slippery surfaces have been achieved, current studies mainly take effect under a contact-type stimulus with restricted working conditions. Most recently, to achieve contact-less manipulation of droplets, photo-thermal responsive slippery surfaces with programmable wettability were developed.[35,36] Under near-infrared or sunlight irradiation, the lubricant state or/and surface wettability were changed, therefore achieving the effective and nimble manipulation of droplets. Of note, the

[a]*School of Chemistry, Beihang University, Beijing 100191, China. E-mail: henglp@buaa.edu.cn; Fax: +86 10-82627566*

[b]*School of Materials Science and Engineering, Zhengzhou University, Zhengzhou 450052, P. R. China*

† Electronic supplementary information (ESI) available. See DOI: 10.1039/d1ta04243b

‡ These authors contributed equally to this work.

above surfaces were principally focused on constructing the surface responsivity by integrating a photothermal material in the whole substrate, which had difficulty in satisfying flexible responsive demands under complicated practical environments. Therefore, a feasible strategy to design a patterned photothermal slippery surface and achieve spatial droplet manipulation remains extremely challenging nowadays.

In this paper, we present a photothermal responsive ZnO–Pt–FAS–paraffin composite slippery surface (ZPFPSS) with patterns and smartly control the sliding behaviour of various liquid droplets under on–off light irradiation. Owing to Pt's photothermal characteristic, the phase-change paraffin endowed the slippery surface with a switchable wettability transition between the easy-sliding state and pinning solid state for various droplets. Assisted by patterned Pt sputtering, the droplet motion can be further spatially manipulated on the versatile responsive pathways. In addition, programmable droplet storage on the ZPFPSS with rewritable property was also achieved. Moreover, the ZPFPSS showed superior long-term stability and photothermal self-healing performance. In comparison with other droplet manipulation methods on responsive SLIPSs, this strategy provided contactless response mode and programmable wettability pathways, which showed promising spatial resolution for manipulating droplet movement. This work demonstrates a potential surface for practical applications in rewritable functional biochips, microfluidics and water-harvesting systems.

Results and discussion

For fabricating photothermal responsive slippery surfaces, a substrate with excellent photothermal characteristics, porous structure, and temperature-responsive phase-transition lubricant are requisite. First, we chose an aligned ZnO nanorod array film as the porous substrate owing to its easy availability and economical properties. ZnO nanorod arrays aligned perpendicular to the indium tin oxide (ITO) substrate were fabricated *via* a hydrothermal method.[37] Next, the composite ZnO–Pt photothermal layer was obtained by depositing Pt nanoparticles on the ZnO arrays. Finally, paraffin, a phase-transition material with a melting point (T_m) of 41–44 °C, was used as the lubricant.[38] The paraffin used here would turn into the liquid state at a mild temperature due to its relatively low melting point, which made the responsive process flexible to be controlled and avoided the energy consumption related to overheating under strong light. In practice, the T_m values of paraffin can be on-demand regulated based on the practical requirements in various applications. Fig. 1a schematically illustrates the fabrication process of the ZnO–Pt–FAS–paraffin slippery surface (ZPFPSS) and the droplet manipulation process in response to light irradiation. The ZnO-nanorod array film was deposited with Pt and then infused with liquefied paraffin to construct the ZPFPSS. In case of $T < T_m$ (room temperature), the paraffin was in the solid state, and the droplet on the ZPFPSS demonstrated an air/liquid/solid three-phase system and was in the Wenzel state.[39] Therefore, the droplets would be pinned on the surface. When irradiation was applied, Pt nanoparticles convert light to heat rapidly, leading to the surface temperature rise of the ZPFPSS. Once $T > T_m$, the paraffin melted to form a molecularly smooth low-adhesion slippery interface, which made the liquid droplet slide easily on this surface. While, if the light was turned off, the paraffin cooled and recovered to a solidified rough state, which caused the droplet to be pinned again. The top-view scanning electron microscopy (SEM) images of the original ZnO-nanorod array and Pt-coated (deposition time, 360 s) ZnO-nanorod array are demonstrated in Fig. 1b and c. After

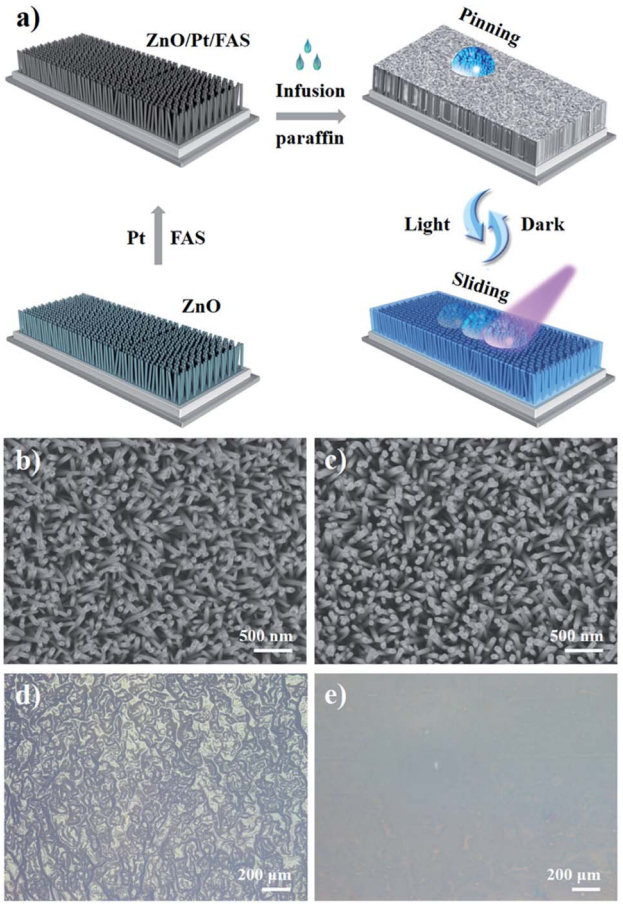

Fig. 1 (a) Schematic demonstration of the ZPFPSS fabrication and intelligent droplet manipulation process through photothermal induced slippery property variation. First, the ZnO-nanopore film was deposited with Pt nanoparticles, then modified with FAS and infused with liquefied paraffin. Without light irradiation, the paraffin on the ZnO–Pt–FAS film was in the solid state and the droplet was pinned on the surface. When light was applied, Pt nanoparticles converted light to heat rapidly inducing $T > T_m$, the paraffin melted into the liquid state and the droplet slid freely on this surface. After the light was turned off, the paraffin cooled and solidified, which caused the droplet to be pinned again. Top-view SEM images of the as-prepared (b) original ZnO-nanopore films with a nanorod average diameter of 54.6 ± 3.4 nm and (c) Pt-coated (deposition time, 360 s) ZnO-nanorod arrays with a diameter of 62.8 ± 4.4 nm. The results show that Pt deposition can slightly increase the diameters of the ZnO nanorods. Real-time microscopy images of paraffin on the ZPFPSS (d) without illumination (room temperature) and (e) under illumination ($T > T_m$), indicating that the rough solid paraffin transformed into a smooth liquefied lubricating layer when the light was on.

depositing Pt, the average diameters of the nanorods slightly increased from 54.6 ± 3.4 nm to 62.8 ± 4.4 nm. The results showed that the nanorods were almost vertical and the morphologies did not change significantly after Pt deposition. The X-ray diffraction pattern of the ZnO nanorod array (Fig. S1†) demonstrated a sharp (002) peak, confirming that the (001) planes of ZnO were parallel to the ITO surface. After modification with FAS, the Zn, O, Pt, F, C and Si atoms of the ZnO–Pt–FAS surface were uniformly distributed on the surface (Fig. S2†), suggestive of successful Pt deposition and FAS modification. Through capillary forces and matching chemistry, the porous Pt deposited ZnO array film can absorb the melted paraffin into its nano-gap structure to form a stable uniformly slippery surface. A real-time microscopy image of paraffin on the ZPFPSS indicated that the solid paraffin surface was rough at room temperature (Fig. 1d). After light illumination for several minutes, the rough paraffin surface transformed into a smooth liquefied lubricant layer when the temperature was above T_m. Under light illumination, the surface temperature of the ZPFPSS increased sharply due to the extraordinary photothermal conversion capacity of Pt nanoparticles, which would induce the phase transformation of paraffin and the morphology change of the ZPFPSS (Fig. S3†).

For a photothermal responsive slippery surface, the temperature change under light illumination is capable of determining the responsive sensitivity. Of note, the surface temperatures of the samples are detected using an infrared camera (Fig. S3†). Therefore, it is possible to optimize the light intensity and distance that could avoid overheating the ZPFPSS and significantly overcome the temperature limitation in practical applications. The infrared image of the ZPFPSS showed a high surface temperature (Fig. S3a†). In contrast, the ZnO–paraffin surface after illumination for 120 s was still weak due to the lack of photothermal conversion material (Fig. S3b†). To obtain the optimal photothermal responsive slippery surface, the surface temperature changes of ZPFPSSs with different Pt sputtering times were systematically investigated. Fig. S4† shows that the Pt deposition can gradually increase the diameters of the ZnO nanorods. As shown in Fig. 2a, under light illumination, the surface temperatures of all the ZPFPSSs were gradually increased, demonstrating excellent photothermal conversion performance. When the surface temperatures reached the melting point of paraffin, the solid paraffin gradually liquefied and the ZPFPSSs transformed into a slippery state. With the increase of Pt sputtering time, the melting times taken for surface temperatures to reach the melting point of paraffin were reduced. Specifically, the melting times were 45, 25, 18 and 15 s for ZPFPSSs with Pt sputtering times of 120, 240, 360 and 480 s (Fig. 2c), respectively. The reduced melting time is due to the increased Pt nanoparticles and improved photothermal conversion performance. The temperature declining processes of the ZPFPSSs were also carefully recorded. As shown in Fig. 2b, the initial temperatures for all ZPFPSSs were set as 60 °C. In air, the surface temperatures of all the surfaces were gradually reduced and the liquid paraffin would convert to a solid when the surface temperatures went below its melting point. The solidification times taken for surface temperatures to

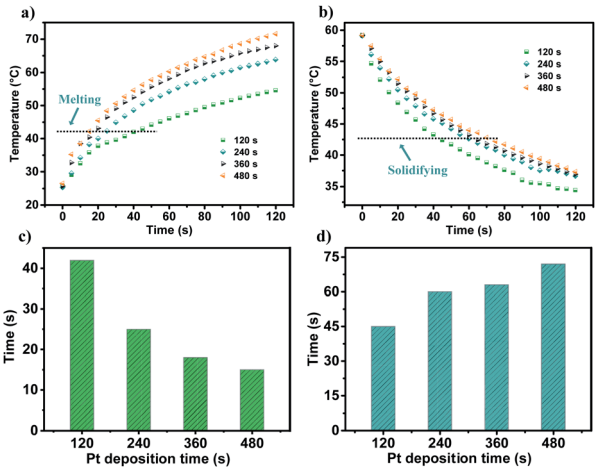

Fig. 2 Temperature change processes of the ZPFPSS with different Pt deposition times under 3 sun illumination with (a) turning on the light (melting process) and (b) turning off the light (solidification process). (c) The time from room temperature to the melting point of paraffin in the ZPFPSS with various Pt deposition times under 3 sun illumination. (d) The time from 60 °C to the solidification point of paraffin in the ZPFPSS with different Pt deposition times. The light intensity is 3 sun.

drop from 60 °C to its melting point were increased with extension of the Pt sputtering time.[35] Specifically, the solidification times were 45, 60, 63 and 72 s for Pt sputtering times of 120, 240, 360 and 480 s (Fig. 2d), respectively. As a control, the temperature change processes of the ZnO–paraffin were also monitored. As shown in Fig. S5,† the surface temperature of ZnO–paraffin was just 32.4 °C after light irradiation for 120 s, which is much lower than that of the ZPFPSS. After comprehensive consideration of the melting time and economic cost, a Pt sputtering time of 360 s was selected in the following experiments unless otherwise stated.

To investigate the surface wettability and slippery properties of the as-fabricated ZPFPSS with switching on/off the light, we measured the contact angles (CAs) and sliding angles (SAs) of water and organic droplets. Before infusing paraffin, the surface wettability of ZnO, ZnO–Pt and ZnO–Pt–FAS films was firstly measured. As shown in Fig. S6,† ZnO and ZnO–Pt films showed excellent hydrophilicity with water CAs of 20.1 ± 1.4° and 18.9 ± 1.5°, respectively. After being modified with FAS, the ZnO–Pt–FAS film demonstrated hydrophobicity with a water CA of 116.7 ± 1.9°. After infusing paraffin, without light irradiation, the droplet CAs on the ZPFSS are 111.2 ± 2.8°, 95.3 ± 2.7°, 89.6 ± 2.1°, 79.2 ± 2.6°, 52.5 ± 3.1°, and 61.8 ± 3.3° for 3 μL water, glycerol, formamide, ethylene glycol (EG), dimethyl phthalate (DMP), and ionic liquid, respectively (Table S1 and Fig. S7a†). After turning on the light source, all the droplet CAs decreased due to the melting of paraffin. Specifically, water, glycerol, formamide, EG, DMP, and ionic liquid showed CAs of 85.2 ± 2.4°, 79.1 ± 2.5°, 76.6 ± 2.9°, 67.2 ± 2.3°, 29.4 ± 2.7° and 51.8 ± 3.0°, respectively. As for a given liquid, the CAs show no obvious change in response to changing the droplet volumes when the light is on and off (Fig. S7b–g†). Similar to the change of CAs, the SAs of various liquids were all decreased after turning on the

light illumination. Specifically, the SAs of 3 μL water, glycerol, formamide, EG, DMP and ionic liquid dramatically decreased from 90°, 60.2 ± 2.7°, 65.0 ± 3.4°, 70.4 ± 3.1°, 76.3 ± 2.9° and 77.1 ± 3.2° under no light irradiation to 6.3 ± 1.4°, 7.2 ± 1.6°, 8.1 ± 1.3°, 7.5 ± 1.8°, 8.8 ± 1.5° and 7.6 ± 1.9° with light irradiation, respectively (Fig. 3a). The above results can be attributed to the reduced friction force caused by the melting of paraffin. Notably, the ZPFPSS exhibited small SAs for liquid droplets with surface tensions from 31.3 to 72.1 mN m^{-1} (Table S1†), suggestive of its omniphobic character. For a predetermined liquid type, the SAs decrease with the increase of the volume. As shown in Fig. 3b–g, the SAs decrease sharply with the increase of droplet volume without light illumination, while the SAs decrease slightly under light illumination. Under light irradiation, the SAs of the various droplets of 3 μL are all smaller than 10°, and further decrease to about ~2.5° when the volume increased to 15 μL, which demonstrated excellent slippery properties. Moreover, the excellent slippery properties of the surface remained (Fig. S8†) after storage under ambient conditions for 180 d without diaphragmation, demonstrating superior long-term stability. Furthermore, the water SA changes on ZPFPSSs with various Pt sputtering times were also studied (Fig. S9†). The water droplets showed almost the same SAs on the above ZPFPSSs, showing no effect of Pt sputtering time on the surface slippery property. We further measured the reversible switching SAs on the ZPFPSS during five cycles with switching on/off the light, which showed superior cycling stability for various types of liquid droplet (Fig. 4). Therefore, the ZPFPSS would demonstrate a switchable slippery property in response to switching on and off the light source.

For explaining the effect of light irradiation on the variations of SAs, the force analysis of a droplet on the tilted surface before and after irradiation is schematically illustrated in Fig. S10,† where N and f represent the support force and friction force, and m_g indicates the gravity of the droplet, which includes two components (F_1, parallel to the surface, and F_2, perpendicular to the surface and equal to N). When $F_1 \geq f$, the droplet would move on the tilted surface. Generally, F_1 is determined by the gravity and the tilt angle, and f is related to the state of paraffin wax.[11] Under the conditions of no light illumination, the paraffin wax is solid, which leads to a large f. Therefore, to drive the droplet sliding on the surface, a large driving force (F_1) and therefore a large tilt angle (α) are needed, which will produce a large SA. When irradiation was applied, Pt nanoparticles converted light to heat rapidly which induced $T > T_m$, and the saturated infused paraffin melted to form a thick lubricating layer with molecular smoothness, low adhesion force and tiny f, and a small tilt angle (β) was needed to propel the droplet sliding, making the liquid droplet slide easily on such surface with small SAs. To quantitatively investigate the force change, the retention forces between the droplets and the surface were detected without and with light illumination. As shown in

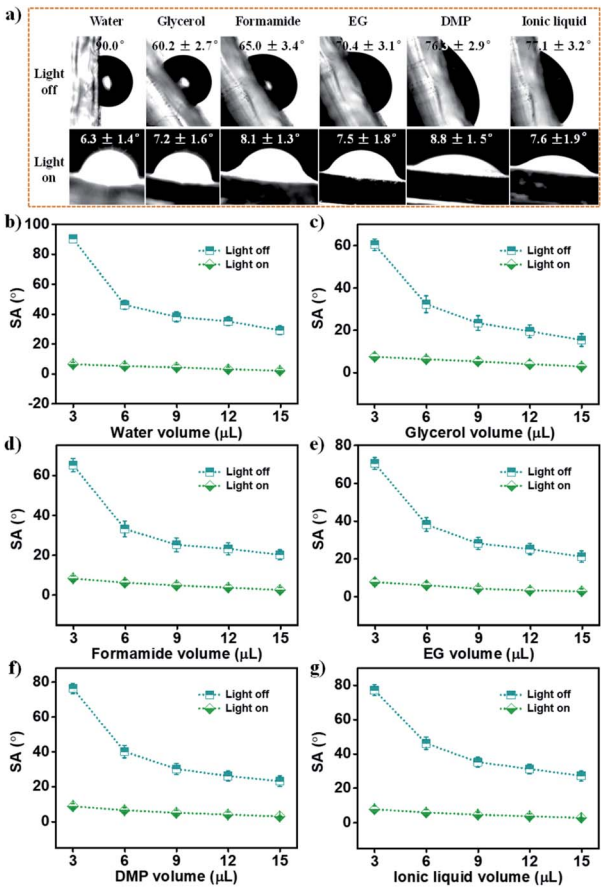

Fig. 3 (a) SA photos of various liquid droplets (3 μL) on the ZPFPSS with light illumination off and on. SA values *vs.* liquid volumes of (b) water, (c) glycerol, (d) formamide, (e) EG, (f) DMP, and (g) ionic liquid with light illumination off and on.

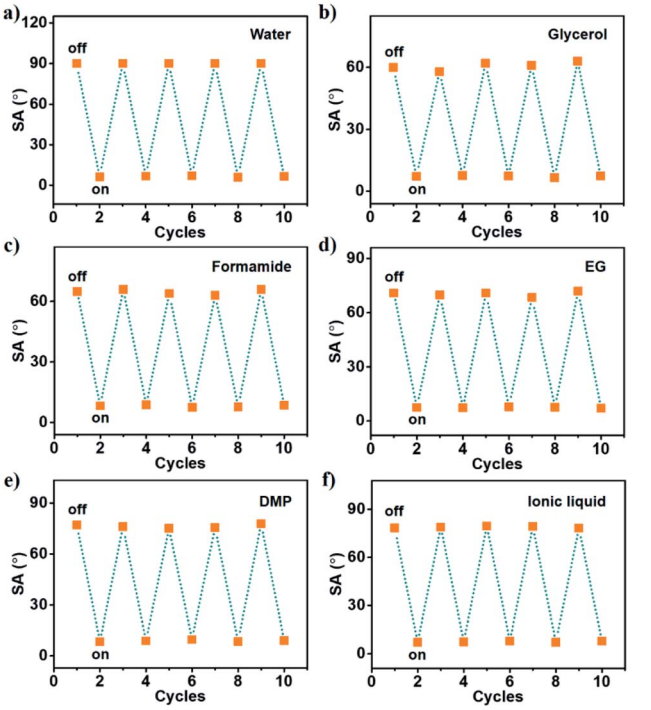

Fig. 4 Liquid droplet SAs reversibly switching on the ZPFPSS in response to switching on/off the light: (a) water, (b) glycerol, (c) formamide, (d) EG, (e) DMP, (f) ionic liquid.

Fig. S11,† before light illumination, the retention forces between the droplets and the surface were 42.9 ± 2.2, 39.5 ± 3.1, 37.3 ± 2.7, 37.8 ± 2.4, 42.1 ± 3.0 and 38.6 ± 2.8 μN for water, glycerol, formamide, EG, DMP and ionic liquid, respectively. However, the retention forces would become small (~5 μN) when the paraffin melted under light illumination. The larger the retention forces, the larger the SAs (Fig. 3a). The retention force result is in good accordance with SA measurements. Moreover, for a given droplet, with increasing its volume from 3 μL to 15 μL, the increased gravity would allow it to slide at a small tilt angle.

The light-regulated slippery properties of the ZPFPSS would provide a promising strategy to dynamically control the droplet movement on the surface. According to the above results, the dynamic ZPFPSS based on the ZnO–Pt composite film demonstrated switchable slippery property between the easy-sliding state and pinning solid state in response to light illumination. To visibly elaborate the regulable properties, the dynamic surface wettability of the ZPFPSS was investigated by recording the sliding behaviours of various liquid droplets (Fig. 5). For example, as shown in Fig. 5a, a water droplet (dyed with methylene blue) would slide on the surface due to its small SA under light illumination. After turning off the light, the droplet kept sliding a short distance and was finally pinned on the surface at 18 s due to its large SA (which is larger than the tilt angle of 6°). Under the conditions of light off, the water droplet would be held in place on the ZPFPSS. After being exposed to light again, the droplet would slide off the surface due to the melting of paraffin. Similarly, the sliding behaviours of other liquid droplets could also be smartly controlled by switching on/off the light (Fig. 5b–f). This on-demand regulable slippery surface endows the ZPFPSS with huge potential in droplet manipulation applications.

The manipulation of liquid droplets has drawn extensive attention from scientific research to industrial application due to its significant implication in smart microfluidic systems.[40,41] Based on the regulable surface wettability features of the photothermal slippery surfaces, we further endowed the ZPFPSS with programmable responsive pathways for manipulating the droplets. To construct the responsive pathways with different patterns (such as "S" or "Y"), the Pt layer was sputtered onto the porous ZnO surface by using masks with hollowed-out "S" and "Y" regions (Fig. 6). As shown in Fig. 6a–d, there are obvious Pt-

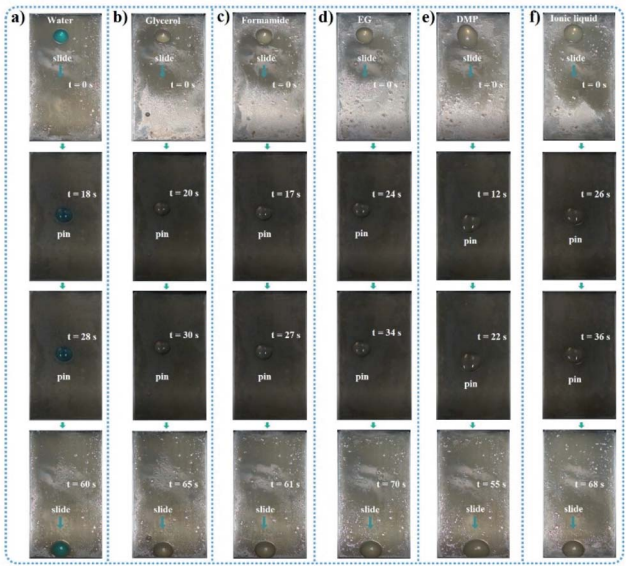

Fig. 5 Demonstration of dynamic control of droplet motion on a tilted ZPFPSS with a tilt angle of ~6°. Droplets were pinned on the surface without irradiation, the droplets slid off the surface after turning on the light irradiation, and the droplets were pinned on the surface again after turning off the light. (a) Water, (b) glycerol, (c) formamide, (d) EG, (e) DMP, and (f) ionic liquid. The volume of the droplets is 9 μL.

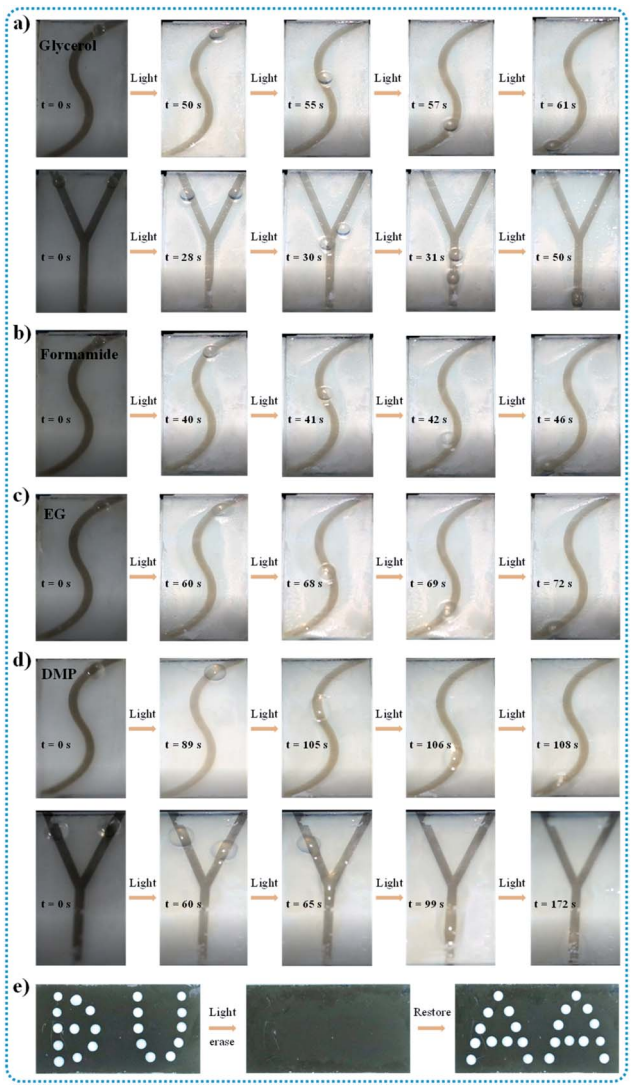

Fig. 6 Time-sequence photographs of continuous droplet sliding and on the ZPFPSS with designed pathways of S-shape pathway and Y-shape pathway, respectively, guided by on–off light illumination. (a) Glycerol, (b) formamide, (c) EG and (d) DMP. (e) Images of patterned droplets sticking on the upright ZPFPSS. On the pristine ZPFPSS, patterns like "B" and "U" letters were presented. After light illumination for 40 s, the droplets slid off the surface, showing excellent erasability. Turning off the light, patterns like letters "A" and "A" could be restored on the surface again.

sputtered "S" and "Y" responsive pathways. After 120 s irradiation, the recorded temperatures of ZPFPSSs with different patterns were much higher in the Pt deposition region (Fig. S3c and d†). Therefore, the paraffin at the pattern regions with Pt and their adjacent area easily melted into a liquid under light irradiation, while it was solid and showed high adhesion at the non-Pt region. Thus, the surfaces with designed wettability pathways could be formed in correspondence with differential light absorption. For instance, as shown in Fig. 6a and Movie S1,† the glycerol droplet was pinned on the surface without light irradiation. After light irradiation for ~50 s, the Pt nanoparticles converted light to heat, and the solid paraffin above the S-shaped pathway gradually melted to the liquid state. As a result, the glycerol droplet slid off the surface along the S-shaped pathway after ~11 s. As for the Y-shaped pathway (Movie S2†), two glycerol droplets were pinned on the surface once they were deposited on the top of the branches. After light illumination for ~28 s, the solid paraffin above the Y-shaped pathway gradually melted to the liquid state, forming a slippery Y-shaped pathway and resulting in the two droplets successively passing the joint point of the branches and then sliding off the surface along the pathway. Similarly, some other droplets (formamide, EG, DMP) can also slide along the S-shaped or Y-shaped pathways under light irradiation (Fig. 6b–d). In addition, DMP droplets were chosen as a specimen to further demonstrate the light-manipulated droplet sliding on the ZPFPSS with designed pathways. As shown in Fig. S12,† the DMP droplets slid freely on the surfaces with an S-shape pathway under light illumination (from 0 s to 9 s). Once the light was turned off, the paraffin would solidify and the friction force increased subsequently. Therefore, the droplets would slow down and finally be pinned on the surfaces (from 15 s to 35 s). When the light was turned on, the paraffin melted and the surface transformed into a slippery state, leading to the sliding of DMP droplets again (from 64 s to 82 s). Similarly, the DMP droplet can also be manipulated on the ZPFPSS with a Y-shape pathway. The above results well confirmed the feasibility of light-manipulated droplet sliding on the ZPFPSS. The responsive pathways endowed the ZPFPSS with spatial droplet manipulation performance.

Moreover, the above reversible surface wettability endowed the photothermal slippery surface with storage and rewritable ability, which can potentially be used as microdroplet patterned chips. As shown in Fig. 3a, the ZPFPSS showed high adhesion towards water droplets even when the surface was vertically positioned under no light irradiation. Therefore, droplets (using milk white dispersion containing 1% polystyrene microparticles for better presentation) stuck on the upright ZPFPSS with patterns like letters "B" and "U" (Fig. 6e). After light irradiation for ~40 s, the patterned droplet letters would easily slide off the surface, showing excellent erasability. When the light was turned off, the surface was restored to the high adhesion state, and letters "A" and "A" could be patterned on the surface again (Fig. 6e). Therefore, this novel ZPFPSS can be flexibly extended to smart microdroplet chips. In comparison with the traditional superhydrophobic surface, another advantage of a slippery surface is its self-healing properties. To investigate the self-healing performance of the ZPFPSS, physical damage was caused by scratching the surface with a sharp blade. As shown in Fig. S12b,† obvious damage lines can be seen on the ZPFPSS. After exposure to light irradiation, the paraffin gradually melted with the increase of surface temperature (Fig. S12c†), and the damage lines disappeared with the replenishment of liquid paraffin to the damage areas (Fig. S12d†). Then, paraffin would gradually solidify with turning off the light and the damage lines completely disappeared (Fig. S12e†), showing no obvious difference with the pristine ZPFPSS (Fig. S12a†). The above experiment indicated that the ZPFPSS possessed outstanding photothermal self-healing performance.

Conclusions

In conclusion, a photothermal responsive ZPFPSS is successfully constructed by integrating surface plasmon resonance Pt nanoparticles, ZnO arrays and a temperature-responsive phase-transition material. Based on the excellent photothermal conversion property of Pt nanoparticles, the paraffin in ZnO nanogaps can be switched between the liquid state and solid state in response to light irradiation. That is to say, the ZPFPSS is endowed with a reversible wettability transition between the easy-sliding state and pinning solid state, therefore achieving the smart manipulation of various droplet sliding behaviours on the surface. By designing a sputtering Pt pattern using different shape masks, the paraffin prefers to melt at the Pt-containing region, which spatially manipulates the sliding pathways of water droplets. In comparison with the reported responsive SLIPSs, this strategy is more flexible and easier to control. Based on the rewritable function, programmable droplet storage on the ZPFPSS was also achieved. Moreover, the ZPFPSS showed superior long-term stability and photothermal self-healing performance. This ZPFPSS demonstrates promising potential in various applications, such as rewritable functional biochips, microfluidics and liquid collection and transfer systems.

Experimental

Materials

All the reagents used in this work were commercially available and used without further treatment. Zinc acetate (99%), zinc nitrate hexahydrate (99%) and 1*H*,1*H*,2*H*,2*H*-perfluorodecyltrimethoxysilane (FAS) (99%) were obtained from J&K Chemicals, China. 2-Methoxyethanol (99%), ethanolamine (99%), hexamethylenetetramine (99%) and paraffin wax (chunks) were purchased from Sigma-Aldrich, China. Formamide, DMP and EG were provided by Aladdin, China. Glycerol was obtained from Xilong Chemical Co., Ltd., China. Methylene blue was purchased from Sinopharm Chemical Reagent Co., Ltd., China. Water (18 MΩ cm) was prepared with a Milli-Q purification system (Millipore Corp., Bedford, MA). The ionic liquid of [OMIm][BF_4] (>99%) was bought from the Lanzhou Institute of Chemical Physics.

Sample preparation

Before preparing the ZnO-nanorod arrays, the ITO substrates were thoroughly cleaned with detergent, deionized water, ethanol, acetone, and deionized water, respectively. Subsequently, the ITO substrates were blow-dried with nitrogen. To fabricate the ZnO-nanorod arrays, a two-step method was adopted as previously reported.[37] First, 0.11 g zinc acetate was dissolved in 1 g 2-methoxyethanol under stirring for 20 min at ambient temperature. After adding 0.0305 g ethanolamine into the above solution and stirring for 2 h, a crystal seed solution with a concentration of 0.5 mol L^{-1} was obtained. Second, to prepare a 0.02 mol L^{-1} growth solution, 2.39 g zinc nitrate hexahydrate and 1.12 g hexamethylenetetramine were dissolved in 400 mL deionized water under stirring for 2 h at room temperature. Third, after spin-coating (KW-4B, China) the crystal seed solution on the ITO substrate and annealing at 270 °C, a thin seed layer was formed on the ITO substrate. Finally, the above ITO substrates with seed layers were suspended in the growth solution. After 6 h of growth at 80 °C, the ITO substates were taken out from the reaction solution, rinsed with water several times and dried at 80 °C for 2 h. Then, the ZnO nanorod arrays were obtained.

To prepare the photothermal substrates, the as-prepared ZnO nanorod arrays were deposited with Pt nanoparticles by a vacuum sputtering method for different times (120 s, 240 s, 360 s, and 480 s, respectively). After being modified with FAS, the photothermal films were infused into the melted paraffin wax at 90 °C for 3 min. After taking out the above films, the excess paraffin was removed by vertically holding the samples for 5 min, and therefore constructing the slippery surfaces.

Characterization

The surface morphology of the sample was observed with a JEOL JSM-7500 (Japan). A Max 2500 X-ray diffractometer with Cu Kα radiation (Rigaku) was used to detect the XRD pattern. The surface wettability and liquid droplet sliding behaviors were characterized by measuring the CAs and SAs with an OCA20 system (Dataphysics, Germany). Given reliability, at least five positions were selected to measure the CAs and SAs on the same sample. The surface tension of DMP was measured using the pendant drop method (OCA20 system). A solar simulator with a xenon arc lamp (CEL-PF300-T8E, Ceaulight, China) equipped with an adjustable aperture (CEL-ND50, Ceaulight) served as the light source. The light intensity was detected *via* an optical power meter (CEL-NP2000-2, Ceaulight). The surface morphology of the paraffin wax on the ZnO–Pt surface at room temperature and under illumination ($T > T_m$) was captured using a microscope (LEXT OLS4500; Olympus, Japan). The retention forces between the liquid droplets and the surface were detected using a surface meter (LSA 100, LAUDA Scientific GmbH). Digital photographs of the droplets sliding on the slippery surface were obtained with a Canon EOS 60D camera.

Conflicts of interest

There are no conflicts to declare.

Acknowledgements

This work was supported by the National Natural Science Foundation of China (21875011, 51922018, 51673010) and the National Key Research and Development Program of China (2017YFA0206904).

References

1 X. Tian, T. Verbo and R. H. A. Ras, *Science*, 2016, **352**, 142–143.
2 Z. Wang, P. Guo, L. Heng and L. Jiang, *Matter*, 2021, **4**, 1274–1286.
3 Z. Sheng, J. Zhang, J. Liu, Y. Zhang, X. Chen and X. Hou, *Chem. Soc. Rev.*, 2020, **49**, 7907–7928.
4 T.-S. Wong, S. H. Kang, S. K. Y. Tang, E. J. Smythe, B. D. Hatton, A. Grinthal and J. Aizenberg, *Nature*, 2011, **477**, 443–447.
5 Z. Wang, L. Heng and L. Jiang, *J. Mater. Chem. A*, 2018, **6**, 3414–3421.
6 Z. F. Gao, R. Liu, J. Wang, J. Dai, W.-H. Huang, M. Liu, S. Wang, F. Xia and L. Jiang, *Chem*, 2018, **4**, 2929–2943.
7 J. Wang, L. Wang, N. Sun, R. Tierney, H. Li, M. Corsetti, L. Williams, P. K. Wong and T.-S. Wong, *Nat. Sustain.*, 2019, **2**, 1097–1105.
8 C. Liu, H. Ding, Z. Wu, B. Gao, F. Fu, L. Shang, Z. Gu and Y. Zhao, *Adv. Funct. Mater.*, 2016, **26**, 7937–7942.
9 P. Guo, Z. Wang, L. Heng, Y. Zhang, X. Wang and L. Jiang, *Adv. Funct. Mater.*, 2019, **29**, 1808717.
10 Q. Rao, A. Li, J. Zhang, J. Jiang, Q. Zhang, X. Zhan and F. Chen, *J. Mater. Chem. A*, 2019, **7**, 2172–2183.
11 Z. Wang, Q. Xu, L. Wang, L. Heng and L. Jiang, *J. Mater. Chem. A*, 2019, **7**, 18510–18518.
12 J. Wang, Y. Huang, K. You, X. Yang, Y. Song, H. Zhu, F. Xia and L. Jiang, *ACS Appl. Mater. Interfaces*, 2019, **11**, 7591–7599.
13 T. Guo, P. Che, L. Heng, L. Fan and L. Jiang, *Adv. Mater.*, 2016, **28**, 6999–7007.
14 Y. Liu, L. Zhao, J. Lin and S. Yang, *Sci. Adv.*, 2019, **5**, eaax0380.
15 C. Chen, Z. Huang, Y. Jiao, L.-A. Shi, Y. Zhang, J. Li, C. Li, X. Lv, S. Wu, Y. Hu, W. Zhu, D. Wu, J. Chu and L. Jiang, *ACS Nano*, 2019, **13**, 5742–5752.
16 Z. Wang, Y. Liu, P. Guo, L. Heng and L. Jiang, *Adv. Funct. Mater.*, 2018, **28**, 1801310.
17 K. Han, L. Heng, Y. Zhang, Y. Liu and L. Jiang, *Adv. Sci.*, 2019, **6**, 1801231.
18 V. C. Mai, S. Hou, P. R. Pillai, T.-T. Lim and H. Duan, *ACS Nano*, 2021, **15**, 6977–6986.
19 Q. Rao, J. Zhang, X. Zhan, F. Chen and Q. Zhang, *J. Mater. Chem. A*, 2020, **8**, 2481–2489.
20 X. Xiao, C. Zhang, H. Ma, Y. Zhang, G. Liu, M. Cao, C. Yu and L. Jiang, *ACS Nano*, 2019, **13**, 4083–4090.
21 Q. Li and Z. Guo, *J. Mater. Chem. A*, 2018, **6**, 13549–13581.
22 L. Hauer, W. S. Y. Wong, V. Donadei, K. I. Hegner, L. Kondic and D. Vollmer, *ACS Nano*, 2021, **15**(3), 4658–4668.

23 K.-C. Park, P. Kim, A. Grinthal, N. He, D. Fox, J. C. Weaver and J. Aizenberg, *Nature*, 2016, **531**, 78–82.
24 W. Liu, X. Luo, C. Chen, G. Jiang, X. Hu, H. Zhang and M. Zhong, *Lab Chip*, 2021, **21**, 1373–1384.
25 X. Yao, Y. Hu, A. Grinthal, T.-S. Wong, L. Mahadevan and J. Aizenberg, *Nat. Mater.*, 2013, **12**, 529–534.
26 J. Kamei and H. Yabu, *Adv. Funct. Mater.*, 2015, **25**, 4195–4201.
27 Y. Huang, B. B. Stogin, N. Sun, J. Wang, S. Yang and T.-S. Wong, *Adv. Mater.*, 2017, **29**, 1604641.
28 M. Cao, X. Jin, Y. Peng, C. Yu, K. Li, K. Liu and L. Jiang, *Adv. Mater.*, 2017, **29**, 1606869.
29 I. Oh, C. Keplinger, J. Cui, J. Chen, G. M. Whitesides, J. Aizenberg and Y. Hu, *Adv. Funct. Mater.*, 2018, **28**, 1802632.
30 J. Wang, L. Sun, M. Zou, W. Gao, C. Liu, L. Shang, Z. Gu and Y. Zhao, *Sci. Adv.*, 2017, **3**, e1700004.
31 J. Li, E. Ueda, D. Paulssen and P. A. Levkin, *Adv. Funct. Mater.*, 2019, **29**, 1802317.
32 S. Zhu, Y. Bian, T. Wu, C. Chen, Y. Jiao, Z. Jiang, Z. Huang, E. Li, J. Li, J. Chu, Y. Hu, D. Wu and L. Jiang, *Nano Lett.*, 2020, **20**, 5513–5521.
33 K. Manabe, T. Matsubayashi, M. Tenjimbayashi, T. Moriya, Y. Tsuge, K.-H. Kyung and S. Shiratori, *ACS Nano*, 2016, **10**, 9387–9396.
34 K. S. Khalil, S. R. Mahmoudi, N. Abu-dheir and K. K. Varanasi, *Appl. Phys. Lett.*, 2014, **105**, 041604.
35 J. Wang, W. Gao, H. Zhang, M. Zou, Y. Chen and Y. Zhao, *Sci. Adv.*, 2018, **4**, eaat7392.
36 C. Gao, L. Wang, Y. Lin, J. Li, Y. Liu, X. Li, S. Feng and Y. Zheng, *Adv. Funct. Mater.*, 2018, **28**, 1803072.
37 D. Tian, Q. Chen, F.-Q. Nie, J. Xu, Y. Song and L. Jiang, *Adv. Mater.*, 2009, **21**, 3744–3749.
38 D. Wu, B. Ni, Y. Liu, S. Chen and H. Zhang, *J. Mater. Chem. A*, 2015, **3**, 9645–9657.
39 X. Yao, J. Ju, S. Yang, J. Wang and L. Jiang, *Adv. Mater.*, 2014, **26**, 1895–1900.
40 J. N. Wilking, V. Zaburdaev, M. D. Volder, R. Losick, M. P. Brenner and D. A. Weitz, *Proc. Natl. Acad. Sci. U. S. A.*, 2013, **110**, 848–852.
41 K.-H. Chu, R. Xiao and E. N. Wang, *Nat. Mater.*, 2010, **9**, 413–417.